LAWRENCE
LIVERMORE
NATIONAL
LABORATORY

LLNL-CONF-843037

Demonstration of a Full-scale Brassboard TES Microcalorimeter Array for the Athena X-IFU

K. Sakai, S. V. Hull, J. S. Adams, S. Beaumont, R. B. Borrelli, J. A. Chervenak, R. S. Cumbee, F. M. Finkbeiner, J. Y. Ha, R. L. Kelley, C. A. Kilbourne, M. A. Leutenegger, J. N. Mateo, H. Muramatsu, F. S. Porter, S. J. Smith, N. A. Wakeham, E. J. Wassell, S. H. Yoon, M. E. Eckart

December 7, 2022

Applied Superconductivity Conference - ASC 2022
Honolulu, HI, United States
October 23, 2022 through October 28, 2022

Disclaimer

Demonstration of a Full-scale Brassboard TES Microcalorimeter Array for the *Athena* X-IFU

K. Sakai, S. V. Hull, J. S. Adams, S. R. Bandler, S. Beaumont, R. B. Borrelli, J. A. Chervenak, R. S. Cumbee, F. M. Finkbeiner, J. Y. Ha, R. L. Kelley, C. A. Kilbourne, M. A. Leutenegger, J. N. Mateo, H. Muramatsu, F. S. Porter, S. J. Smith, N. A. Wakeham, E. J. Wassell, S. H. Yoon, and M. E. Eckart

***Abstract*—We have characterized a full-scale transition-edge sensor (TES) microcalorimeter array as a milestone towards the demonstration of technology readiness level (TRL) 5 for the detector array for the X-ray Integral Field Unit (X-IFU) instrument on ESA's future flagship X-Ray Observatory called Athena. We fabricated a 90 mm full-scale prototype TES array and measured the properties and the performance in a newly developed platform in which up to 960 out of ~3,200 pixels can be read out. In this paper, we report on measurements of the uniformity of the transition temperature and shape, the uniformity of the spectral energy resolutions at 7 keV and 10 keV, the thermal crosstalk for the first, the diagonal, and the second nearest neighbors, and the energy sensitivities to environment perturbations for the magnetic field, the TES bias voltage, and the heat bath temperature.**

***Index Terms*—X-ray spectroscopy, superconducting device, imaging array, multiplexed readout, transition-edge sensor, Athena space telescope.**

I. Introduction

THE X-ray Integral Field Unit (X-IFU) of European Space Agency's (ESA) Advanced Telescope for High-ENergy Astrophysics (ATHENA) is an X-ray imager and spectrometer, which consists of an array of thousands of transition-edge sensor (TES) microcalorimeters [1]. The TES utilizes the superconducting transition-edge of the sensor material for its very high sensitivity to temperature to enable very high energy resolution, such as ~2 eV for 7 keV X-ray photons. At NASA Goddard Space Flight Center, we are developing the TES array for the X-IFU to provide to the ESA.

We are currently conducting the technology demonstration for Technology Readiness Level (TRL) of 5 [2], and for the first time we have developed a full-scale X-IFU brassboard prototype TES array for the demonstration. The main TRL-5 requirements to the brassboard detector array are:

1. <2.086 eV full-width half-maximum (FWHM) at 7 keV for a sub-set of more than 100 pixels.
2. <4 eV FWHM at 10 keV for a sub-set of pixels.
3. ±0.4 eV uncertainty for 1.5–7 keV in the energy scale calibration for a sub-set of more than 100 pixels.
4. Thermal crosstalk:
   - <0.04% for the first neighbor.
   - <0.03% for the diagonal neighbor.
   - <0.013% for the second and further neighbor.
5. Sensitivity of the energy gain scale (E) to the environment at 7 keV:
   - $\mathrm{d}E/\mathrm{d}B$ < 3 eV/nT for the magnetic field.
   - $\mathrm{d}E/\mathrm{d}V_{\mathrm{bias}}$ < 15 meV/ppm for the TES bias voltage (V_{bias}).
   - $\mathrm{d}E/\mathrm{d}T_{\mathrm{b}}$ < 0.15 eV/μK for the heat bath temperature (T_{b}).

Although the baselined readout method for X-IFU is time-division multiplexing (TDM) [3]–[5], these detector-level requirements are at the component level and should not include

This material is based upon work supported by NASA under award number 80GSFC21M0002 and is supported in part by an appointment to the NASA Postdoctoral Program at the NASA Goddard Space Flight Center, administered by Oak Ridge Associated Universities under contract with NASA. (Corresponding author: K. Sakai, e-mail: Kazuhiro.Sakai@nasa.gov)

K. Sakai, J. S. Adams, and N. A. Wakeham are with Center for Space Sciences and Technology, University of Maryland, Baltimore County, Baltimore, MD 21250 and NASA Goddard Space Flight Center (GSFC), Greenbelt, MD 20771, USA.

S. V. Hull is a NASA Postdoctoral Program Fellow, NASA GSFC, Greenbelt, MD 20771

S. Beaumont is with Center for Space Sciences and Technology, University of Maryland, Baltimore County, Baltimore, MD 21250, IRAP, 9 Avenue du Colonel Roche, 31400 Toulouse, France, and NASA GSFC, Greenbelt, MD 20771, USA.

R. S. Cumbee is with University of Maryland, College Park, MD 20742 and NASA GSFC, Greenbelt, MD 20771, USA.

F. M. Finkbeiner is with Sigma Space Corp. / Hexagon US Federal, 4600 Forbes Blvd., Lanham, MD 20706, USA and NASA GSFC, Greenbelt, MD 20771, USA.

J. Y. Ha is with SB Microsystems, 806 Cromwell Park Dr, Glen Burnie, MD 21061, USA and NASA GSFC, Greenbelt, MD 20771, USA.

H. Muramatsu is with the Catholic University of America, Washington, DC 20064, USA and NASA GSFC, Greenbelt, MD 20771, USA.

S. Yoon is with Science Systems and Applications, Inc. (SSAI) 10210 Greenbelt Rd, Lanham, MD 20706, USA and NASA GSFC, Greenbelt, MD 20771, USA.

S. R. Bandler, R. B. Borrelli, J. A. Chervenak, R. L. Kelley, C. A. Kilbourne, M. A. Leutenegger, J. N. Mateo, F. S. Porter, S. J. Smith, and E. J. Wassell are with NASA GSFC, Greenbelt, MD 20771, USA

M. E. Eckart is with Lawrence Livermore National Laboratory, Livermore, CA 94550, USA.

Color versions of one or more of the figures in this paper are available online at http://ieeexplore.ieee.org.

Digital Object Identifier will be inserted here upon acceptance.

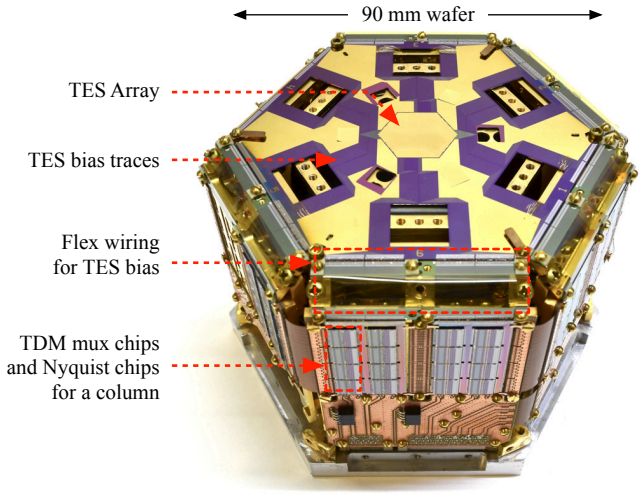

Fig. 1. A photograph of the 960-pixel detector assembly. On the side panels, 10 out of 24 total columns are populated for the readout of 400 pixels at maximum. The 90-mm detector wafer is kinematically mounted on the snout assembly with 3 sapphire balls and Cu clips. The detector wafer and the readout circuits on the sides are connected via Kapton flex with superconducting Nb traces.

contributions from performance degradation from the TDM. Therefore, all the measurements in this study were carried out either in a non-multiplexed way or in a slow and low-number TDM multiplexing.

In this study, we will discuss the measurement results that demonstrate the ability to meet (1), (2), (4), and (5) of the above TRL-5 requirements. The requirement (3) is discussed in [6].

II. Detector Design and Measurement Setup

A. X-IFU Detector Design

The current baseline X-IFU detector consists of an array of 2,376 TESs with a pixel pitch of 317 μm, tiled in a hexagonal shape covering a 5-arcminute field-of-view. Each TES is a 50 × 50 μm^2 Mo/Au bilayer and has a cantilevered Au/Bi absorber with an additional Au finish to increase infrared reflectivity, with the size close to the pixel pitch. The TES pixel design is optimized for the baselined readout method of TDM, and the baselined values are normal resistance (R_n) of 8.8 mΩ, heat capacity (C) of 0.73 pJ/K at 90 mK, and thermal conductance (G_b) of 72 pW/K at 90 mK. More details of the TES design are discussed in [7]. With this pixel design, we have achieved combined spectral energy resolutions of 1.95 eV for Ti-Kα (4.5 keV), 1.97 eV for Mn-Kα (5.9 keV), 2.16 eV for Co-Kα (6.9 keV), 2.33 eV for Cu-Kα (8 keV), and 3.26 eV for Br-Kα (11.9 keV) for >200 pixels with 8-column by 32-row TDM on a 32 × 32 pixel array, which all meet the broad-band resolution requirements [8].

The developed prototype TES array studied in this work has 3,168 pixels, and 936 pixels of them are wired out to the bonding pads sitting along the perimeter of a 90-mm hexagonal wafer chip. The pixels are fabricated on 275 μm pitch. The TES bilayer is 42 nm Mo and 223 nm Au. The absorber size is 268 × 268 × 4 μm^3 with thickness 3.1 μm Bi and 1.3 μm Au. The number of pixels is larger, and the absorbers are slightly smaller and more densely packed than the current design of X-IFU since this version of prototype array is based on a previous baseline X-IFU.

B. Measurement Setup

The prototype array was measured in our 960-pixel platform, which is capable of 24-column × 40-row TDM readout. The cooler is an adiabatic magnetization refrigerator (ADR) backed by He^3. The 55-mK detector assembly is hexagonally shaped and has six side panels. The 90-mm prototype TES array is mounted at the top surface as shown in Fig. 1. Each side panel can have up to 4-columns of the TDM SQUID-1 (SQ1) multiplexing chips and the Nyquist inductor (640 nH) chips mounted to it. The Nyquist inductor chip also carries the TES shunt resistances (79 μΩ). The TES array and the side panels are connected via Kapton flexes with superconducting Nb traces [9].

In this prototype a variety of slightly different designs of TDM SQ1 multiplexing chips [5] were used in the setup. Special care was needed to ensure that the needed operating parameters of the different chips, such as the row switching voltage, were all the same where multiple columns were fed from single signal lines. The second stage SQUIDs [10] were placed at the 3K temperature stage of the ADR.

Due to the limited availability of the TDM multiplexing chips, we have so far populated 10 columns out of the 24 total columns available, which allows readout of up to 400 TES pixels. However, ~10 rows were not accessible due to defects in the wire-bonds. In addition, ~100 TES pixels were also not accessible due to defects of the wire-bonds between the prototype array and the Kapton flexes.

The low-noise analog amplifiers were provided by NIST [11]. The rest of the room-temperature electronics used in the measurements are a single-channel analog flux locked loop (FLL) electronics and a commercial-off-the-shelf (COTS) version of TDM digital electronics, built by our group [12]. The TDM digital electronics consists of a Xilinx KCU105 Field Programmable Gate Array (FPGA) evaluation board and 2 GSFC124 ADC/DAC daughter cards. Each evaluation board can read out 4-columns by 40-rows. As stated earlier, the TRL-5 demonstration does not require a multiplexed readout, and the requirements are defined for a non-multiplexed readout. Details of the TDM readout of these types of pixels in a 1k test array are reported in [8]. Therefore, most of the measurements were performed in a non-multiplexed way. For some of the measurements, such as the spectral resolution measurement and the crosstalk measurement, were performed using a slow speed TDM, where the row time (t_{row}) is 800 ns, which is 5-times slower than the standard full-speed TDM, with the maximum number of 4 rows. This allows to reduce the impact of white readout noise, which scales as $\sqrt{N_{row}}$ where N_{row} is the number of rows, and noise from settling transients from the fast TDM row switching.

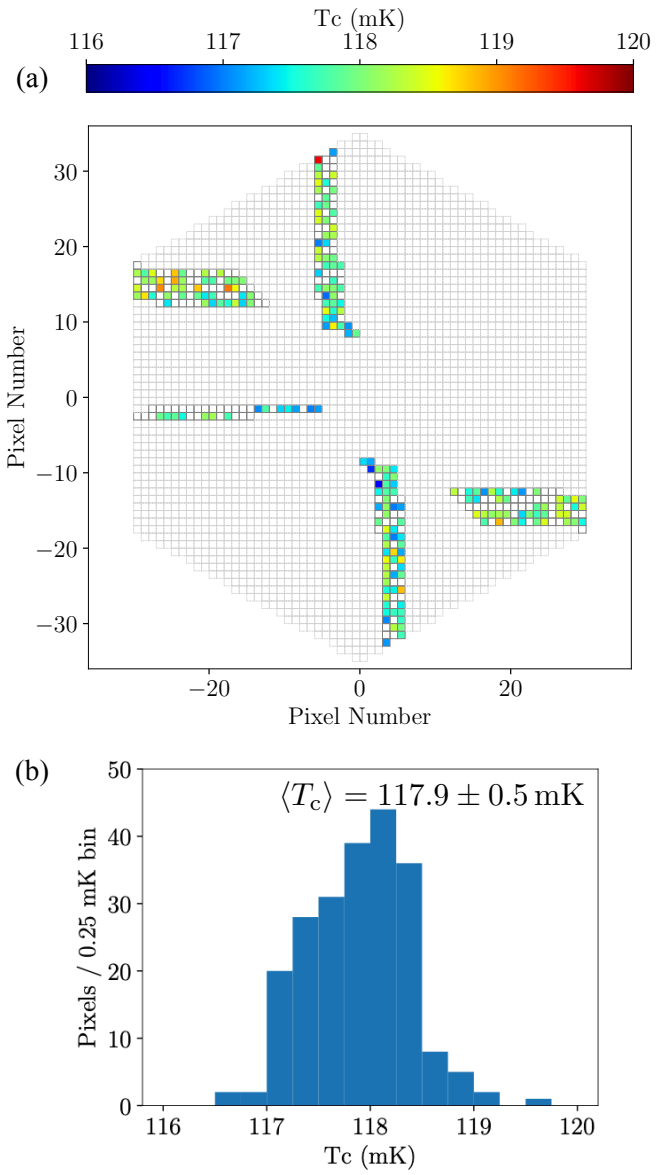

Fig. 2. (a) A heat map of the low TES-bias current transition temperatures for 218 measured pixels (colored pixels). The pixels with the solid line are of the 10 connected columns, covering a large extent of the array. The pixels with the dashed line are of the rest of the columns and therefore not connected. (b) The histogram of the transition temperatures for the measured 218 pixels. The mean is $\langle T_c \rangle = (117.9 \pm 0.5)$ mK.

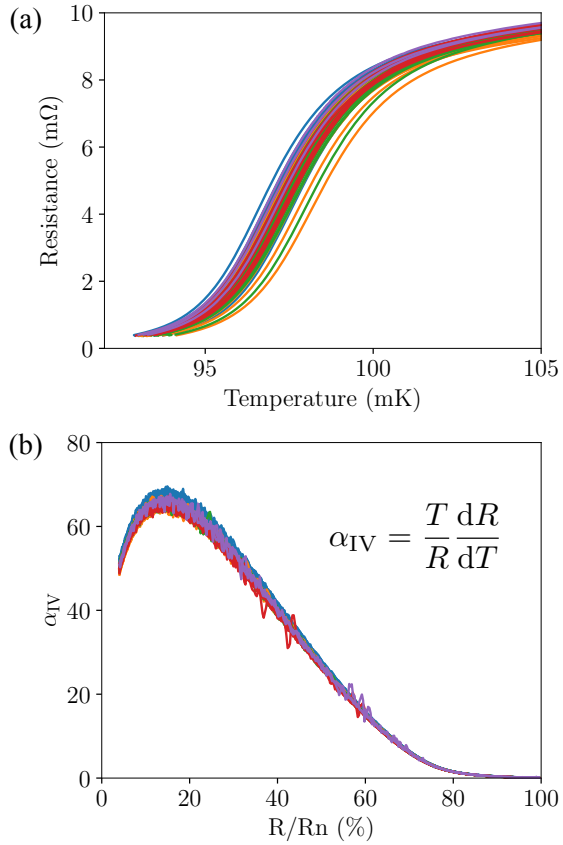

Fig. 3. (a) TES resistances as a function of the TES temperature and (b) α_{IV} as a function of R/R_n for 60 pixels. A few tiny 'kinks' seen in α_{IV} are due to a noise in the measurement.

III. Measurement Results

A. Transition Uniformity

The TES transition temperatures in a low TES-bias current (~10 μA) were measured for 218 pixels. Fig. 2 (a) shows the heat map of the low-bias current transition temperatures and its histogram. The mean transition temperature is $\langle T_c \rangle = (117.9 \pm 0.5)$ mK. Most pixels were uniform in T_c, within approximately a 2 mK range.

The compensating field for the offset field was also measured for each pixel during this measurement. We have seen a linear gradient of the offset field, −0.13 to −0.06 uT, from one side of the array to the other. In the following measurements, we have used the measured value in single pixel measurement and the averaged value for the pixels under test in multiplexed measurement.

We then measured TES $I(V)$ curves for 60 pixels, where I is the TES current and V is the voltage across the TES. Fig. 3 (a) shows the TES resistance (R) as a function of the TES temperature, derived from the power balance equation $I^2R = G_b(T^n - {T_b}^n)/(nT^{n-1})$, where T is the TES temperature, T_b is the heat bath temperature, and n is the exponent of power flow to the heat bath. The measured thermal conductance is uniform across the wafer, and the single representative thermal conductance is $G_b = 86.58$ pW/K at the TES transition temperature of 98.14 mK with $n = 3.4$ where G was determined from a series of I-V measurements at different bath temperatures [7]. The heat bath temperature for the transition curves shown in Fig. 3 (a) was T_b = 55 mK. Fig. 3 (b) shows a plot the $\alpha_{IV} = (TdR)/(RdT)$ as a function of the TES bias point R/R_n, where R_n is the TES normal resistance. Despite the ~2 mK range of transition temperatures, which is consistent with the low TES-bias transition temperature measurement, α_{IV} are largely indistinguishable showing a very uniform pixel responsivity over a large extent of the array.

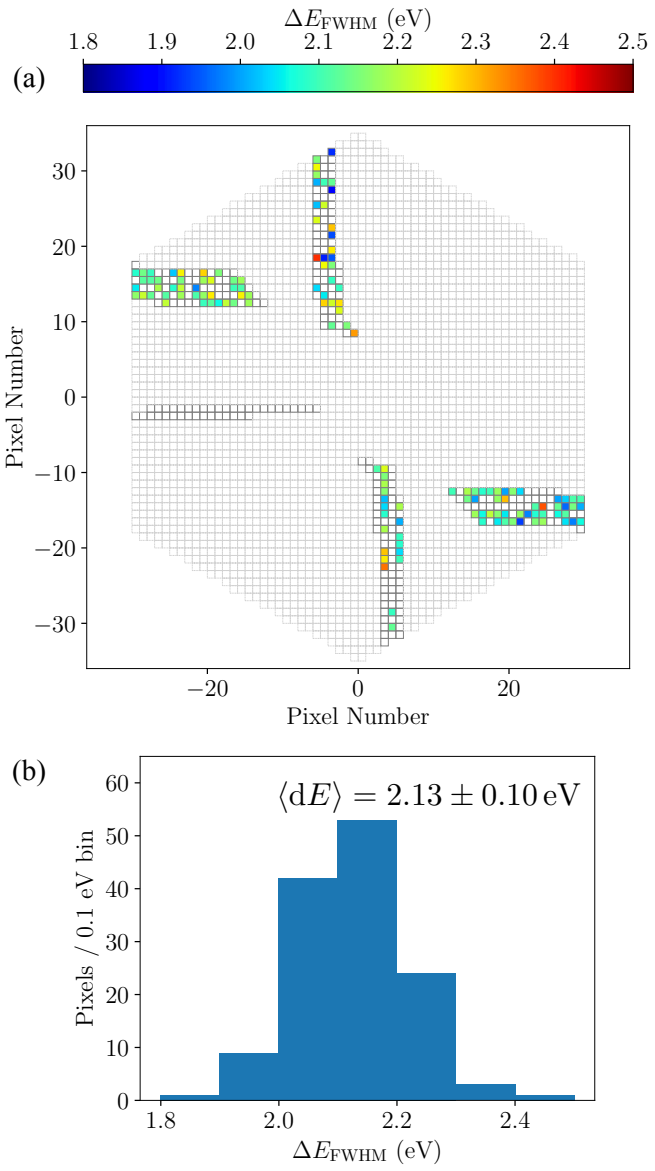

Fig. 4. (a) A heat map of the spectral energy resolution at 7 keV for 134 measured pixels (colored pixels). (b) The histogram of the spectral energy resolutions for the measured 134 pixels. The mean is $\langle \mathrm{d}E \rangle = (2.13 \pm 0.10)$ eV FWHM at 7 keV.

B. *Spectral Energy Resolution*

The spectral energy resolutions ($\mathrm{d}E$) were measured at 7 keV (Co-Kα) at the TES bias point of R/R_{n} = 10% for 134 pixels. For each spectrum, we have collected ~10,000 pulses for the Co-Kα emission line and fitted the line model to obtain the spectral energy resolution. Fig. 4 (a) shows the heat map of the measured energy resolutions for 63 pixels across the large extent of the detector array. Fig. 4 (b) shows the histogram of the energy resolutions, and the mean is $\langle \mathrm{d}E \rangle = (2.13 \pm 0.10)$ eV FWHM at 7 keV. For the given 2.086 eV FWHM at 7 keV requirement, 75% of pixels are within this requirement considering the statistical error of ± 0.1 eV for the individual spectral fitting.

Since the energy resolution scales with $T^{3/2}$, reducing the transition temperature of currently 95 mK at 10% R/R_{n} to the baselined 89 mK would improve the energy resolution by ~0.2 eV, which would allow 95% of the pixels to meet the requirement even without considering the fitting statistical error.

10 keV spectral energy resolutions at Ge-Kα were also measured at the same TES bias point of R/R_{n} = 10% for 15 pixels. The mean is $\langle \mathrm{d}E \rangle = (2.56 \pm 0.07)$ eV FWHM at 10 keV, which is much less than the 4-eV requirement.

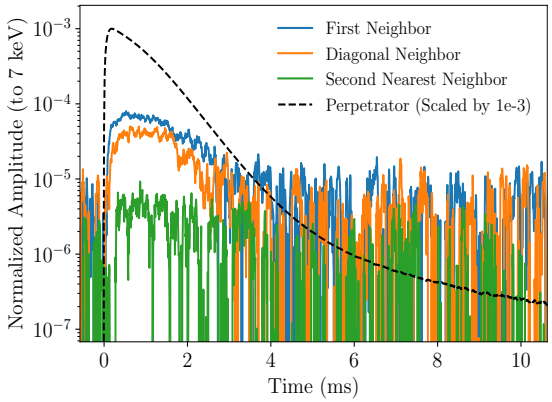

Fig. 5. The extracted thermal crosstalk signals for the first neighbor (blue), the diagonal neighbor (orange), and the second neighbor (green) shown along with the 7-keV *perpetrator* pulse shape (black/dashed) scaled by 10^{-3}. All pulse heights were normalized to the 7keV pulse heights for the corresponding pixel.

C. *Thermal Crosstalk*

The thermal crosstalk was measured using 7 keV pulses. In this measurement, 1 pixel of one column was used as a '*perpetrator*' and 3 neighbor pixels of another column were used as '*victim*.' Those 3 *victim*s are (a) the first neighbor (FN) located below the *perpetrator*, (b) the diagonal neighbor (DN) located at the lower left diagonal from the *perpetrator*, and (c) the second neighbor (SN) located below the first neighbor.

The measured crosstalk signal includes all types of crosstalk that are the electrical crosstalk, which is mainly due to the inductively coupled signal along the signal lines, the TDM-specific crosstalk, which is a crosstalk from a row to the next row, and the thermal crosstalk, which is a thermal crosstalk via the Si frame of the detector chip. Since we are running the TDM at the slow speed, the TDM-specific crosstalk is negligible, but the electrical crosstalk is non-negligible and generally dominates the overall crosstalk, and therefore it needs to be canceled to extract the thermal crosstalk. To cancel the electrical crosstalk, we have conducted two measurements, one with the positive and the other one with the negative polarity TES bias currents. In this way, two measurements exhibit opposite polarity electrical crosstalk (and the TDM-specific crosstalk) while keeping the same polarity for the thermal crosstalk, allowing to cancel the electrical crosstalk if we take the average of the two measured crosstalk signals.

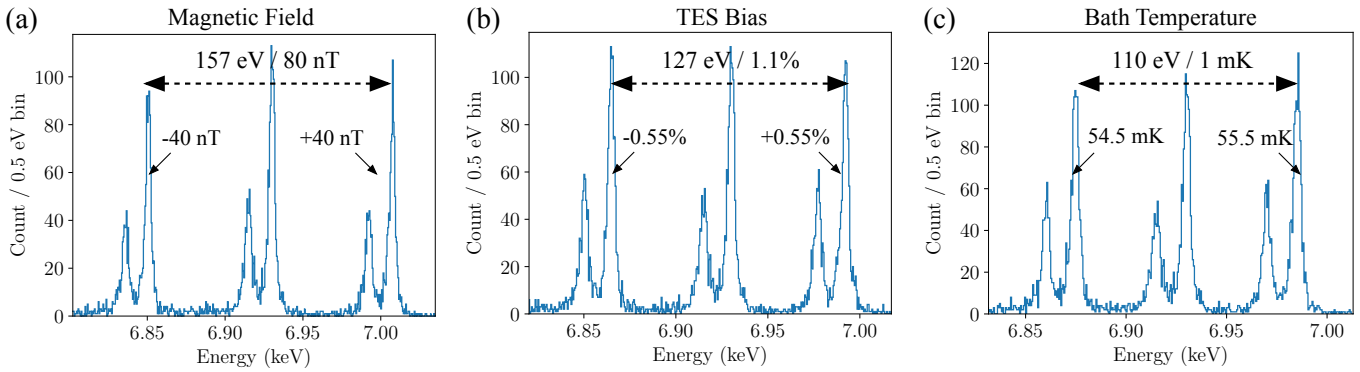

Fig. 6. (a) CoKα line spectra for a single representative pixel, one with the optimal magnetic field located at the center, and two with the perturbated magnetic fields (±40 nT) shifted toward left and right from the center. (b) The same for the nominal TES bias voltage and the perturbated bias voltages (±0.55%). (c) The same for the nominal heat bath temperature and the perturbated bath temperatures (±0.5 mK).

Fig. 5 shows the extracted thermal crosstalk for FN, DN, and SN along with the *perpetrator* pulse scaled by 10^{-3}, all normalized to its own 7-keV pulse heights. The approximate levels of the thermal crosstalk are 0.008% for FN, 0.005% for DN, and <0.001% for SN. These all meet the requirements that are <0.04% for FN, <0.03% for DN, and <0.013% for SN.

D. Environmental Sensitivity

The sensitivities of the energy gain scale to the environmental perturbations for the magnetic field, the TES bias voltage, and the heat bath temperature were measured at 7 keV for 12 pixels. For each measurement, we have collected ~2,000 pulses for the Co-Kα emission line, which makes the statistical error for the line energy centroid to be ~±0.06 eV. For the magnetic field, we have applied ±40 nT from the optimal magnetic field that makes the low-bias transition temperature the largest. For the TES bias voltage, we have varied ±0.55%. For the heat bath temperature, we have varied ±0.5 mK. These perturbations cause ±50—100 eV shift of the line energy centroid.

Fig. 6 shows the shifts of the Co-Kα lines for a single representative pixel for (a) the magnetic field, (b) the TES bias voltage, and (c) the heat bath temperature perturbations. For the measured 12 pixels, the mean sensitivities are $\langle \mathrm{d}E/\mathrm{d}B \rangle = 2.1 \pm 0.1$ eV/nT for the magnetic field, $\langle \mathrm{d}E/\mathrm{d}V_{\mathrm{bias}} \rangle = 11.7 \pm 0.2$ meV/ppm for the TES bias voltage, and $\langle \mathrm{d}E/\mathrm{d}T_{\mathrm{b}} \rangle = 0.108 \pm 0.002$ eV/μK for the heat bath temperature, and these are all meeting the requirements, including the maximum sensitivities of 2.3 eV/nT, 11.9 meV/ppm, and 0.118 eV/μK for $\mathrm{d}E/\mathrm{d}B$, $\mathrm{d}E/\mathrm{d}V_{\mathrm{bias}}$, and $\mathrm{d}E/\mathrm{d}T_{\mathrm{b}}$ respectively.

IV. Summary

We have fabricated the X-IFU full-scale prototype TES array and measured the properties and the performances of the array for the TRL-5 milestone. The array was measured on our 960-pixel test platform and our results showed a uniform low-bias Tc distribution across the wafer, as well as uniform transition shapes and α_{IV}. The mean spectral energy resolution at 7 keV for 134 pixels is $\langle \mathrm{d}E \rangle = (2.13 \pm 0.10)$ eV FWHM. If the transition temperature is reduced to the baselined 89 mK, it is expected that 95% of measured pixels are meeting the requirement without considering the fitting statistical error. 10 keV mean spectral energy resolution for 15 pixels is $\langle \mathrm{d}E \rangle = (2.56 \pm 0.07)$ eV FWHM, which satisfies the requirement of 4 eV with a large margin. We have also measured thermal crosstalk and environmental sensitivity for the magnetic field, TES bias voltage, and heat bath temperature, and all the results meet the requirements.

References

[1] D. Barret et al., "The Athena X-ray Integral Field Unit: a consolidated design for the system requirement review of the preliminary definition phase," accepted for publication in Experimental Astronomy (2022), doi: 10.48550/arXiv.2208.14562.

[2] NASA, "Technology Readiness Level Definitions," https://www.nasa.gov/pdf/458490main_TRL_Definitions.pdf

[3] J. A. Chervenak, K. D. Irwin, E. N. Grossman, J. M. Martinis, C. D. Reintsema, and M. E. Huber, "Superconducting multiplexer for arrays of transition edge sensors," *Appl Phys Lett*, vol. 74, no. 26, pp. 4043–4045, Jun. 1999, doi: 10.1063/1.123255.

[4] W. B. Doriese *et al.*, "Developments in Time-Division Multiplexing of X-ray Transition-Edge Sensors," *J Low Temp Phys*, vol. 184, no. 1–2, pp. 389–395, 2016, doi: 10.1007/s10909-015-1373-z.

[5] M. Durkin *et al.*, "Mitigation of Finite Bandwidth Effects in Time-Division-Multiplexed SQUID Readout of TES Arrays," *IEEE T Appl Supercon*, vol. 31, no. 5, 2021, doi: 10.1109/tasc.2021.3065279.

[6] S. J. Smith *et al.*, "Correcting Gain Drift in TES Detectors for Future X-ray Satellite Missions," these proceedings.

[7] A. R. Miniussi *et al.*, "Performance of an X-ray Microcalorimeter with a 240 μm Absorber and a 50 μm TES Bilayer," *J Low Temp Phys*, vol. 193, no. 3–4, pp. 337–343, May 2018, doi: 10.1007/s10909-018-1974-4.

[8] S. J. Smith *et al.*, "Performance of a Broad-Band, High-Resolution, Transition-Edge Sensor Spectrometer for X-ray Astrophysics," *IEEE T Appl Supercon*, vol. 31, no. 5, 2021, doi: 10.1109/tasc.2021.3061918.

[9] J. A. Chervenak *et al.*, "Broadside-coupled niobium flexible cables," these proceedings

[10] R. P. Welty and J. M. Martinis, "Two-stage integrated SQUID amplifier with series array output," *IEEE T Appl Supercon*, vol. 3, no. 1, pp. 2605–2608, 1993, doi: 10.1109/77.233523.

[11] C. D. Reintsema *et al.*, "Electronics for a Next-Generation SQUID-Based Time-Domain Multiplexing System," *AIP Conference Proceedings*, vol. 1185, pp. 237–240, 2009, doi: 10.1063/1.3292321.

[12] K. Sakai *et al.*, "Developments of Laboratory-Based Transition-Edge Sensor Readout Electronics Using Commercial-Off-The-Shelf Modules," *J Low Temp Phys*, 2022, doi: 10.1007/s10909-022-02810-z.

Acknowledgement: Part of this work was performed under the auspices of the U.S. Department of Energy by Lawrence Livermore National Laboratory under Contract DE-AC52-07NA27344.